Spin crossover equation of state and sound velocities of $(Mg_{0.65}Fe_{0.35})O$ ferropericlase to 140 GPa

Bin Chen,[1,2] Jennifer M. Jackson,[1] Wolfgang Sturhahn,[1] Dongzhou Zhang,[1] Jiyong Zhao,[3] June K. Wicks,[4] and Caitlin A. Murphy[1]

Received 21 January 2012; revised 6 July 2012; accepted 13 July 2012; published 30 August 2012.

[1] We have determined the elastic and vibrational properties of periclase-structured $(Mg_{0.65}Fe_{0.35})O$ ("FP35"), a composition representative of deep mantle "pyrolite" or chondrite-pyroxenite models, from nuclear resonant inelastic x-ray scattering (NRIXS) and x-ray diffraction (XRD) measurements in diamond-anvil cells at 300 K. Combining with *in situ* XRD measurements, the Debye sound velocity of FP35 was determined from the low-energy region of the partial phonon density of states (DOS) obtained from NRIXS measurements in the pressure range of 70 to 140 GPa. In order to obtain an accurate description of the equation of state (EOS) for FP35, separate XRD measurements were performed up to 126 GPa at 300 K. A new spin crossover EOS was introduced and applied to the full *P-V* data set, resulting in a zero-pressure volume $V_0 = 77.24 \pm 0.17$ Å^3, bulk modulus $K_0 = 159 \pm 8$ GPa and its pressure-derivative $K'_0 = 4.12 \pm 0.42$ for high-spin FP35 and $K_{0,LS} = 72.9 \pm 1.3$ Å^3, $K_{0,LS} = 182 \pm 17$ GPa with $K'_{0,LS}$ fixed to 4 for low-spin FP35. The high-spin to low-spin transition occurs at 64 ± 3 GPa. Using the spin crossover EOS and Debye sound velocity, we derived the shear (V_S) and compressional (V_P) velocities for FP35. Comparing our data with previous results on (Mg,Fe)O at similar pressures, we find that the addition of iron decreases both V_P and V_S, while elevating their ratio (V_P/V_S). Small amounts (<10%) of low-spin FP35 mixed with silicates could explain moderate reductions in wave speeds near the core mantle boundary (CMB), while a larger amount of FP35 near the CMB would not allow a large structure to maintain neutral buoyancy.

Citation: Chen, B., J. M. Jackson, W. Sturhahn, D. Zhang, J. Zhao, J. K. Wicks, and C. A. Murphy (2012), Spin crossover equation of state and sound velocities of $(Mg_{0.65}Fe_{0.35})O$ ferropericlase to 140 GPa, *J. Geophys. Res.*, *117*, B08208, doi:10.1029/2012JB009162.

1. Introduction

[2] Knowledge of the sound velocities and density of lower mantle minerals are essential for interpreting seismic complexity in the deep Earth. The Earth's lower mantle accounts for nearly half of the mass and volume of the planet. Iron (Fe) is the most abundant transition metal in the lower mantle, and it is hosted mainly by silicate perovskite, post-perovskite and ferropericlase. The spin-pairing crossover of Fe from the high-spin (HS) to low-spin (LS) state in Fe-poor periclase-structured (Mg,Fe)O, referred to here as "ferropericlase", has been recognized to affect the density and sound velocities of this second most abundant lower mantle phase [e.g., *Antonangeli et al.*, 2011; *Badro et al.*, 2003; *Crowhurst et al.*, 2008; *Komabayashi et al.*, 2010; *Lin et al.*, 2005, 2006; *Marquardt et al.*, 2009; *Speziale et al.*, 2005; *Wentzcovitch et al.*, 2009; *Wu et al.*, 2009; *Zhuravlev et al.*, 2009]. An enhanced Fe content is found to significantly reduce the sound velocities of periclase [*Wicks et al.*, 2010], which may be a source of ultra-low velocity zones (ULVZs) above the core mantle boundary (CMB) [e.g., *Bower et al.*, 2011; *Garnero and Helmberger*, 1995; *McNamara et al.*, 2010; *Wicks et al.*, 2010]. High-pressure and high-temperature elastic and vibrational properties of ferropericlase with various Fe contents are thus of significant importance for interpreting seismic complexity in terms of compositional variations [*Goncharov et al.*, 2006; *Mattern et al.*, 2005] and for constructing geodynamic models with suitable candidate phases [*Bower et al.*, 2009, 2011]. However, experimental studies of the sound velocities of ferropericlase have not been fully explored in pressure-temperature-composition space. Ferropericlase may be Fe-rich

[1]Seismological Laboratory, California Institute of Technology, Pasadena, California, USA.
[2]Now at Department of Earth and Environmental Sciences, University of Michigan, Ann Arbor, Michigan, USA.
[3]Advanced Photon Source, Argonne National Laboratory, Argonne, Illinois, USA.
[4]Division of Geological and Planetary Sciences, California Institute of Technology, Pasadena, California, USA.

Corresponding author: B. Chen, Department of Earth and Environmental Sciences, University of Michigan, Ann Arbor, MI 48109, USA. (binchen@umich.edu)

0148-0227/12/2012JB009162

compared with silicate perovskite and post-perovskite [*Fei et al.*, 1996; *Fiquet et al.*, 2010; *Murakami et al.*, 2005; *Sakai et al.*, 2009; *Sinmyo et al.*, 2008; *van Westrenen et al.*, 2005]. In the lowermost 200 km of the lower mantle, namely the *D″* layer, Fe has been shown to enter preferentially into ferropericlase, in comparison with post-perovskite, thus leading to the plausible existence of Fe-rich ferropericlase [e.g., *Auzende et al.*, 2008; *Kobayashi*, 2005; *Sakai et al.*, 2009].

[3] Knowing the details of lower mantle mineralogy requires, in part, thermoelastic data for lower mantle constituents at relevant conditions. To date, considerable efforts have been focused on measuring the density and sound velocities of candidate mantle minerals under high-pressure and high-temperature conditions [e.g., *Antonangeli et al.*, 2011; *Crowhurst et al.*, 2008; *Jackson et al.*, 2004, 2006; *Lin et al.*, 2006; *Mao et al.*, 2011; *Murakami et al.*, 2009; *Murakami and Bass*, 2011]. However, only a few measurements exist that probe the sound velocities of minerals under lower mantle conditions. Recent developments in Brillouin spectroscopy and impulsive stimulated light scattering (ISLS) using diamond-anvil cells have enabled measurements of the sound velocities of Earth materials that are transparent or translucent in the visible wavelength regime. Specifically, the aggregate compressional (V_P) and shear (V_S) wave velocities of polycrystalline aluminous $MgSiO_3$ perovskite have been measured up to 40 GPa [*Jackson et al.*, 2004] and V_S of polycrystalline MgO and $MgSiO_3$-perovskite and post-perovskite have been determined up to 130, 96, and 172 GPa, respectively [*Murakami et al.*, 2007a, 2007b, 2009]. Using ISLS, the body wave velocities of $(Mg_{0.94}Fe_{0.06})O$ have been determined up to 60 GPa, revealing significant softening over the pressure range from 40 to 60 GPa [*Crowhurst et al.*, 2008]. More Fe-rich compositions are typically opaque to visible light, rendering x-ray scattering methods such as inelastic x-ray scattering (IXS) and nuclear resonant inelastic X-ray scattering (NRIXS) a more suitable tool. It should be noted that the ISLS technique can also be used to determine sound velocities of opaque materials [*Crowhurst et al.*, 2004]. Using NRIXS, the Debye sound velocity (V_D) of $(Mg_{0.75}Fe_{0.25})O$ has been determined up to 110 GPa at 300 K [*Lin et al.*, 2006], indicating lower V_P and V_S of this ferropericlase compared to MgO. Also using NRIXS, *Wicks et al.* [2010] found V_S of $(Mg_{0.16}Fe_{0.84})O$ at 120 GPa to be 50% lower than that of the preliminary reference Earth model (PREM) at the same pressure [*Dziewonski and Anderson*, 1981], lending credit to Fe-rich (Mg,Fe)O-bearing ULVZs above the CMB [*Bower et al.*, 2011; *Wicks et al.*, 2010]. Sound velocities of single-crystal $(Mg_{0.83}Fe_{0.17})O$ obtained from the measured dispersion curves by IXS [*Antonangeli et al.*, 2011] manifest enhanced shear elastic anisotropy across the spin transition of Fe, which is consistent with Brillouin scattering measurements on single-crystal $(Mg_{0.9}Fe_{0.1})O$ up to 69 GPa [*Marquardt et al.*, 2009].

[4] The amount of Fe contained in the periclase-structured $(Mg_{0.65}Fe_{0.35})O$, referred to as "FP35" hereafter, studied here is within the estimated range for a "pyrolite" lower mantle [e.g., *Sinmyo et al.*, 2008; *van Westrenen et al.*, 2005] and an aluminum-poor chondrite-pyroxenite lower mantle [e.g., *Fei et al.*, 1996; *Irifune*, 1994]. By comparing the elastic and vibrational properties of this candidate lower mantle component with seismic models such as PREM [*Dziewonski and Anderson*, 1981] under relevant *P-T* conditions, one could gain a better understanding of the composition and structure of the Earth's deep mantle. In this study, we measured the ^{57}Fe-weighted partial phonon density of states (DOS) and volume of FP35 by simultaneous NRIXS and *in situ* X-ray diffraction (XRD) measurements in panoramic diamond-anvil cells. We present a spin crossover EOS to fit our separate XRD data up to 126 GPa for the same FP35 sample. Using our spin crossover EOS, we derived V_P and V_S from the V_D determined from the low-energy region of the DOS.

2. Experimental Methods

[5] The ^{57}Fe-enriched FP35 sample was synthesized from powders of $^{57}Fe_2O_3$ (95% enriched) and fired MgO in a H_2/CO_2 gas-mixing furnace at 1673 K and $\log f_{O_2} = -9$ for approximately 20 hours. The sample was then reground and heated for another 20 hours. The synthesized FP35 sample was analyzed using a JEOL JXA-8200 electron microscope, indicating a composition of $(Mg_{0.654(1)}Fe_{0.330(1)}Ti_{0.016(1)})O$, where the numbers in parentheses indicate the uncertainties in the last digit of atomic weight. This analysis also revealed a chemically homogeneous polycrystalline sample at the length scale investigated and an absence of metallic Fe, with the latter confirmed by synchrotron Mössbauer spectroscopy measurements. The Ti in the sample was found to originate from the $^{57}Fe_2O_3$ starting material purchased from AMT Ventures Ptd Ltd. This amount of Ti in FP35 is unlikely to have a significant affect on V_D, based on NRIXS measurements of wüstite (FeO) with and without Ti. At ambient conditions, we find $V_D = 2.88 \pm 0.01$ km/s for $Fe_{1-x}O$ with $\rho = 6.05 \pm 0.03$ g/cm^3 and $V_D = 2.87 \pm 0.01$ km/s for $(Fe_{0.959}Ti_{0.041(1)})O$ with $\rho = 5.99 \pm 0.06$ g/cm^3.

[6] High-pressure NRIXS and XRD experiments were conducted at Beamline 3-ID-B of the Advanced Photon Source (APS) at Argonne National Laboratory, and the storage ring was operated in the top-up mode with 24 bunches that were separated by 153 ns [*Sturhahn*, 2004]. For these experiments, two panoramic DACs with beveled 250 and 150-μm flat culet diamonds were prepared. The panoramic DACs have a 90° axial opening slot, which was positioned in the downstream direction of the x-rays. A cubic boron nitride backing plate was placed on this end of the DAC to observe XRD of the sample at 14.4125 keV. A sample chamber close to the culet size was drilled out of a pre-indented beryllium gasket with a typical indentation thickness of 40 μm and was filled with a boron epoxy insert to maintain sample thickness at high pressures and reduce the axial pressure gradient [*Lin et al.*, 2003]. The sample, with a typical size of 20-30 μm in diameter and $\sim$10 μm thick, was loaded in a hole that was either laser- or mechanically drilled within the boron epoxy insert. Neon was loaded into the sample chamber as the pressure medium for the DAC with 250-μm flat anvils, using the gas loading system at GeoSoilEnviroCARS (Sector 13) at the APS [*Rivers et al.*, 2008] and our gearbox customized for the panoramic diamond-anvil cell. Ruby spheres were used as initial pressure markers. XRD data were collected *in situ* at Beamline 3-ID-B before and after each set of NRIXS measurements at the same sample position for a given compression point, in order to determine the unit-cell volume. The final

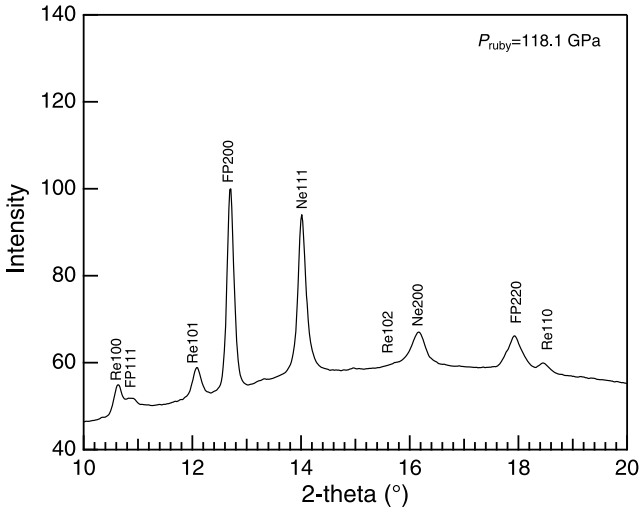

Figure 1. A typical XRD pattern of FP35 at 118.1 GPa and 300 K. The *hkl* indices for FP35 (FP), rhenium (Re), and neon (Ne) are labeled above each peak.

reported pressures in this study were assigned using the new spin crossover EOS for FP35 (see Section 3.1), by averaging the volumes of FP35 determined from the *in situ* XRD measurements. The typical pressure drift during NRIXS measurements was less than 2 GPa at 105 GPa and ~4 GPa at 140 GPa.

[7] High-energy-resolution NRIXS spectra were obtained by tuning the x-ray energy around the nuclear transition energy of ^{57}Fe at 14.4125 keV. Three avalanche photodiode detectors (APDs) were positioned radially around and proximal to the sample in order to collect the incoherent inelastic scattered photons [*Sturhahn*, 2004]. A fourth APD was positioned downstream in the forward scattering direction and independently measured an average energy resolution of 1.2 meV at the FWHM [*Toellner*, 2000]. The high-resolution monochromator was tuned around the nuclear resonance energy of ^{57}Fe with a step size of 0.25 meV and a collection time of 3 to 5 s per energy step. NRIXS spectra were collected at five compression points from 70 to 140 GPa, and the scanned energy range varied depending on the pressure.

[8] Separate XRD measurements of FP35 were performed at Beamline 12.2.2 of the Advanced Light Source (ALS), Lawrence Berkeley National Laboratory, using an incident energy of 30 keV (λ = 0.41328 Å). A grain of FP35 from the same bulk sample as used for the NRIXS measurements was loaded in a DAC with beveled 250-μm culet diamond anvils. Rhenium was used for the gasket and the pressure medium was neon. Ruby spheres were used as pressure markers and the ruby fluorescence spectra were of good quality up to the highest pressure (P_{ruby} = 125.8 GPa [*Jacobsen et al.*, 2008]). A MAR3450 image plate was used to collect the diffraction images and the FIT2D software was used to integrate the diffraction patterns. Small pressure increments were taken in order to resolve the volume collapse resulting from the spin crossover of Fe in the sample. Due to the large tails of the focused x-ray beam at Beamline 12.2.2, every x-ray pattern contains diffraction peaks from the rhenium gasket. At low pressure, the (200), (311), (220) and (400) reflections are well-resolved. However, at P < 20 GPa, the (111) and (200) reflections of FP35 overlap with the (100) and (101) reflections of rhenium. Despite that, at least 3 reflections from FP35 were used in deriving its lattice parameter as a function of pressure at each compression point. A typical XRD pattern is shown in Figure 1.

3. Results

3.1. Spin Crossover Equation of State

[9] In some XRD reports on the *P-V* trend of (Mg,Fe)O, the HS and LS states of B1-structured (Mg,Fe)O have been treated separately by two independent EOS [*Fei et al.*, 2007; *Lin et al.*, 2005]. This approach does not reproduce the behavior in the crossover region (typically around 60 GPa) and introduces uncertainties of elastic parameters based on the particular choice of pressure regions representative of HS and LS states. The crossover region which extends typically between 40 GPa and 80 GPa and in which spin states may co-exist requires a more detailed description. A linear-superposition approach that combines two Birch-Murnaghan EOS for HS or LS states according to their thermal occupation number has provided a good reproduction of the crossover region in some situations [*Crowhurst et al.*, 2008; *Mao et al.*, 2011]. We will take a similar approach and construct our spin crossover EOS starting with the Helmholtz free energy of the material given by an elastic and a spin contribution

$$F(V,T) = F_{\text{elastic}} + F_{\text{spin}}. \tag{1}$$

We impose additional constrains by requiring that $p = -(\partial(F_{\text{elastic}} + F_{\text{HS}})/\partial V)_T$ and $p = -(\partial(F_{\text{elastic}} + F_{\text{LS}})/\partial V)_T$ are Birch-Murnaghan EOS for HS or LS states, respectively, albeit with different parameter sets. Vibrational contributions become important at higher temperatures but may be neglected in the present treatment aimed at describing data taken at room temperature. For the elastic contribution, we choose an expression corresponding to the commonly used third-order Birch-Murnaghan EOS

$$F_{\text{elastic}} = \frac{9}{2} V_0 K_0 f^2 \left\{1 + \left(K_0' - 4\right) f\right\}, \tag{2}$$

where the Eulerian strain is given by $f = \{(V_0/V)^{2/3} - 1\}/2$. The three empirical parameters describing the shape of the compression curve are the zero-pressure values of volume, V_0, bulk modulus, K_0, and pressure derivative of the bulk modulus, K_0'.

[10] The contribution of the 3d electrons of the Fe atoms in a mineral is captured here by a simplified version, neglecting spin-spin interactions, of an expression for F_{spin} introduced earlier [*Sturhahn et al.*, 2005]

$$F_{\text{spin}} = V_0 n \sum_i E_i \eta_i + V_0 \frac{n}{\beta} \sum_i \eta_i \ln \frac{\eta_i}{g_i}, \tag{3}$$

where n is the zero-pressure number density of Fe atoms and $\beta = 1/(k_B T)$ is the inverse temperature. Each Fe atom can occupy energetically different 3d-electron states described by an index i with energy E_i and degeneracy g_i. For the occupation probabilities of these states, η_i, we assume a "spin equilibrium", i.e., $\eta_i = g_i \exp(-\beta E_i)/Z$ with $Z = \sum_j g_j \exp\left(-\beta E_j\right)$. The combination of (1), (2), and (3) then

Table 1. Compression Data of FP35 at 300 K in a Neon Pressure Medium From XRD Measurements[a]

P[b] (GPa)	V(Å^3)	ρ[c] (g/cm^3)	P (GPa)	V(Å^3)	ρ (g/cm^3)
1 bar	77.79(30)	4.383(17)	64.8(2)	59.34(30)	5.745(29)
5.0(1)[d]	74.43(36)	4.581(23)	67.5(3)	58.57(29)	5.821(29)
9.7(3)	72.75(36)	4.686(24)	70.1(3)	58.35(29)	5.843(30)
12.2(1)	72.25(35)	4.719(24)	72.5(3)	57.36(29)	5.943(30)
14.9(1)	7114(35)	4.793(24)	75.1(7)	57.03(29)	5.978(30)
18.7(1.6)	70.36(35)	4.846(24)	78.1(3)	56.58(29)	6.025(30)
20.1(1)	69.69(35)	4.892(25)	80.3(4)	56.23(28)	6.064(31)
23.3(1)	69.24(34)	4.924(25)	82.2(7)	55.84(28)	6.106(31)
27.2(2)	68.07(34)	5.009(25)	85.2(4)	55.60(28)	6.132(31)
29.8(3)	67.15(33)	5.078(26)	87.6(3)	55.17(27)	6.180(31)
32.0(1)	66.63(33)	5.117(26)	90.6(4)	54.84(27)	6.217(31)
35.0(2)	65.78(32)	5.183(26)	95.4(1.0)	54.68(27)	6.235(32)
38.7(2)	65.11(46)	5.236(37)	101.8(4)	53.85(27)	6.331(32)
44.3(2)	63.86(32)	5.339(27)	105.2(3)	53.47(27)	6.376(32)
49.3(2)	62.86(31)	5.424(27)	109.5(5)	53.04(26)	6.428(32)
53.2(7)	61.99(31)	5.500(28)	114.1(5)	52.61(26)	6.481(33)
57.3(7)	61.12(31)	5.578(28)	118.1(6)	52.16(26)	6.537(33)
61.4(3)	59.88(30)	5.694(29)	125.8(7)	51.68(26)	6.598(33)

[a]The measurements were conducted at beamline 12.2.2 at the Advanced Light Source, Lawrence Berkeley National Laboratory.
[b]Pressures were determined from fluorescence spectra of small ruby spheres loaded close to the sample in a neon pressure medium [*Jacobsen et al.*, 2008].
[c]Density is determined by the measured volume and the chemical formula given in section 2, using 95% ^{57}Fe.
[d]The numbers in parentheses are uncertainties. Pressure: standard deviation of the pressures determined from the ruby fluorescence spectra collected before and after each XRD measurement. Volume: estimated to be ~0.5%. Density: error propagation.

provides the EOS via $p = -(\partial F/\partial V)_T$. This EOS has the following material-dependent parameters: energy levels of the 3d-electron states E_i, their volume dependence, and their degeneracies g_i; zero-pressure number density of Fe atoms n; zero-pressure volume V_0, bulk modulus K_0, and bulk modulus derivative K'_0 for the HS and LS states. Whereas zero-pressure number density of Fe atoms can be determined from composition and zero-pressure volume, values for the energy levels are difficult to obtain. They could, for example, be calculated in a more fundamental theoretical description of the material. In the spirit of a more simple empirical approach, we decided to model the energy levels and their volume dependence with as few parameters as possible. We assume that all energy levels can be expressed as multiples of the difference between crystal field splitting, Δ, and spin pairing energy, Λ. For example, the energy of the LS state is given by $E_{LS} = a_{LS}(\Delta - \Lambda)$ and at very high pressures $F_{spin} = V_0 n E_{LS}$. The requirement that the compression curves for HS and LS states are described by Birch-Murnaghan EOS constrains the volume dependence of $(\Delta - \Lambda)$ according to

$$\Delta - \Lambda = \omega_0 + \frac{1}{nV_0 a_{LS}}\left(F_{elastic}^{(LS)} - F_{elastic}^{(HS)}\right), \quad (4)$$

where $F_{elastic}^{(HS)}$ and $F_{elastic}^{(LS)}$ are calculated with (2) and parameters specific to HS and LS states. The volume independent parameter ω_0 determines the transition pressure (p_{tr}) as the spin crossover occurs close to $\Delta = \Lambda$.

[11] We applied our spin crossover EOS to describe the P-V relation of FP35. In the calculation of the compression curve, we varied the following set of parameters: HS zero-pressure volume V_0; HS zero-pressure bulk modulus K_0; HS zero-pressure bulk modulus derivative K'_0; LS zero-pressure volume $V_{0,LS}$; LS zero-pressure bulk modulus $K_{0,LS}$; LS zero-pressure bulk modulus derivative $K'_{0,LS}$; transition parameter ω_0. The number of Fe atoms in the unit cell, nV_0, is determined by the measured composition of our sample.

[12] The symmetry of the Fe site was assumed to be perfectly octahedral which allowed us to use $a_{HS} = 0$, $g_{HS} = 15$ for the HS state, $a_{IS} = 1$, $g_{IS} = 18$ for the intermediate-spin state, and $a_{LS} = 2$, $g_{LS} = 1$ for the LS state. Jahn-Teller distortions which are expected to be present in the environment of HS Fe^{2+} would partially lift the degeneracy of the HS state and could be included in our model by using an appropriate spread of values for a_{HS}. For the present data set, this refinement was not required to obtain an excellent fit to the measured compression curve.

[13] The compression data of FP35 measured at 300 K (Table 1) has been fit using the spin crossover EOS as described above. We obtain for the HS zero-pressure volume $V_0 = 77.24 \pm 0.17$ Å^3, the HS zero-pressure bulk modulus $K_0 = 159 \pm 8$ GPa, and the HS zero-pressure derivative of the bulk modulus $K'_0 = 4.12 \pm 0.42$, where the uncertainties are reported at the 2σ level (Figure 2). These values are in very good agreement with past reports on the zero-pressure elasticity of (Mg,Fe)O with similar Fe concentrations [*Fei et al.*, 1992; *Jacobsen et al.*, 2002; *Jackson et al.*, 2006; *Lin et al.*, 2005; *van Westrenen et al.*, 2005; *Zhuravlev et al.*, 2009]. Furthermore, we obtained a LS zero-pressure volume of $V_{0,LS} = 72.9 \pm 1.3$ Å^3 and a LS zero-pressure bulk modulus of $K_{0,LS} = 182 \pm 17$ GPa with the LS zero-pressure derivative of the bulk modulus fixed at $K'_{0,LS} = 4$. From analysis of the normalized pressure (F) versus strain (f) [e.g., *Angel*, 2001], one can see that K'_0 is consistent with the data (Figure 2a). However, even though $K'_{0,LS}$ was constrained to 4 in the LS region, one can see the influence of the spin transition region (Figure 2a).

[14] In an effort to compare with previous investigations that report two different EOS for the HS and LS states, we use our spin EOS formalism to fit end-member HS and LS scenarios that avoid the transition region (Figure 2a). The resulting parameters with associated uncertainties from our fits (see Figure 2a) are in good agreement with those reported by *Fei et al.* [2007] for a similar composition. Specifically, *Fei et al.* [2007] used powder x-ray diffraction to investigate the P-V behavior of a suite of (Mg,Fe)O samples with variable Fe concentrations, using NaCl as a pressure medium. For their $(Mg_{0.61}Fe_{0.39})O$ sample, the composition closest to that investigated here, they report the following parameters from their two separate Birch-Murnaghan EOS (HS: V_0 fixed to 77.48 Å^3, $K_0 = 156 \pm 2$ GPa, K'_0 fixed to 4; LS: $V_{0,LS} = 73.6 \pm 0.1$ Å^3, $K_{0,LS} = 170 \pm 3$ GPa, and $K'_{0,LS}$ fixed to 4).

[15] In the thermodynamic description used here, a single EOS is used to fit all the data through the crossover. Therefore, we also obtain information on the characteristics of the spin crossover in FP35, namely the volume dependence of $(\Delta - \Lambda)$ and the transition pressure $p_{tr} = 64 \pm 3$ GPa determined at the 50 % level of the volume collapse across the spin transition. The volume dependence of $(\Delta - \Lambda)$ following from (4) is an excellent approximation described by $\Lambda = 1.82$ eV and $\Delta = \Delta_0(V_0/V)^{\xi}$ with $\Delta_0 = 1.45$ eV and $\xi = 0.91$. At the spin crossover, we observe a volume collapse of 2.1 Å^3 corresponding to 2.7 % of the HS zero-pressure volume and 3.6 % of the volume at the transition pressure. The fit to the FP35 compression data by our spin crossover EOS suggests a

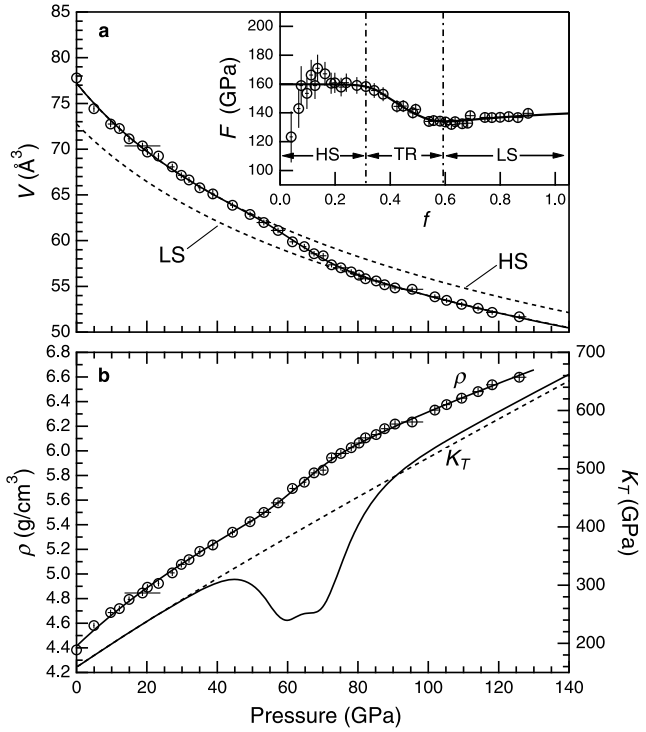

Figure 2. Compression behavior of FP35 across the HS-LS transition at 300 K. (a) Volume data of FP35 up to 126 GPa are fit using the spin crossover EOS described in Section 3.1 (solid black line: V_0 = 77.24 ± 0.17 Å^3, K_0 = 159 ± 8 GPa, K'_0 = 4.12 ± 0.42, $V_{0,LS}$ = 72.9 ± 1.3 Å^3, $K_{0,LS}$ = 182 ± 17 GPa, and $K'_{0,LS}$ fixed to 4). Using the same spin EOS, the dashed curves represent fits only to the HS region, 0 to 38.7 GPa (dashed upper curve: V_0 = 77.23 ± 0.23 Å^3, K_0 = 160 ± 11 GPa, and K'_0 = 4.05 ± 0.60) and LS region, 80.3 to 125.8 GPa (dashed lower curve: $V_{0,LS}$ = 72.76 ± 0.60 Å^3 and $K_{0,LS}$ = 184.0 ± 8.5 GPa, with $K'_{0,LS}$ fixed to 4). The upper right inset shows normalized pressure (F) as a function of strain (f) of our EOS (solid curve) and the measured data (open circles with errors). HS, high-spin state; TR, spin crossover transition region; LS, low-spin state. (b) Density of FP35 and K_T (solid curve) as a function of pressure, showing a minimum in K_T at 64 ± 3 GPa. Dashed curve shows K_T for HS FP35.

minimum in the bulk modulus at p_{tr}, exhibiting up to 38 % softening in the bulk modulus.

3.2. Sound Velocities

[16] The PHOENIX software (Version 2.0.0) was used to derive the partial phonon DOS of FP35 from the NRIXS spectra by removing the elastic contribution and applying the quasi-harmonic lattice model [*Sturhahn*, 2000] (Figure 3). The Debye sound velocity, V_D, was determined from the low-energy region of the DOS using the psvl module in PHOENIX [*Jackson et al.*, 2009; *Sturhahn and Jackson*, 2007] and the density from the spin crossover EOS. For an isotropic solid, the seismically relevant aggregate V_p and V_S can be calculated from the following two equations $3/V_D^3 = (1/V_P^3) + (2/V_S^3)$ and $V_P^2 - \frac{4}{3}V_S^2 = K_S/\rho$ [*Sturhahn and Jackson*, 2007], where K_S is the adiabatic bulk modulus and ρ is the density. K_S can be approximated by the isothermal bulk modulus K_T, because $K_S = K_T(1 + \alpha\gamma T)$ and $\alpha\gamma T < 0.01$ at room temperature. The values for K_T from the spin crossover EOS of FP35 were used to derive V_P and V_S (see Figure 2b). The determined seismically relevant velocities V_P and V_S from 70 to 140 GPa at 300 K are shown in Figure 4 and Table 2. The shear modulus, G, can be calculated from $\rho V_S^2 = G$. It is important to note that V_S is typically more constrained than V_P, because V_S is less dependent on the choice of EOS [*Sturhahn and Jackson*, 2007]. As we report the complete *P-V* EOS and determine the volume of the sample *in situ*, the density and hence, G and V_P of FP35 are also well constrained in this study.

[17] It is also important to note that for crystals with cubic symmetry, as is the case for FP35, the phonon DOS is isotropic. The NRIXS method directly provides the Fourier-transformed self-intermediate scattering function, $S(k, E)$. The dependence of $S(k, E)$ on the direction of the incident x-rays has been discussed previously [*Sturhahn and Kohn*, 1999] and is expressed via the directional dependence of the phonon DOS. The potential anisotropy of the phonon DOS should not be confused with the elastic anisotropy: the description of the former is given by a symmetric second-rank tensor [e.g., *Sturhahn and Kohn*, 1999; *Sturhahn and Jackson*, 2007], whereas the latter requires a symmetric fourth-rank tensor. Therefore, in crystals with cubic symmetry, the phonon DOS is isotropic, even though the elastic anisotropy could be large [*Antonangeli et al.*, 2011; *Marquardt et al.*, 2009].

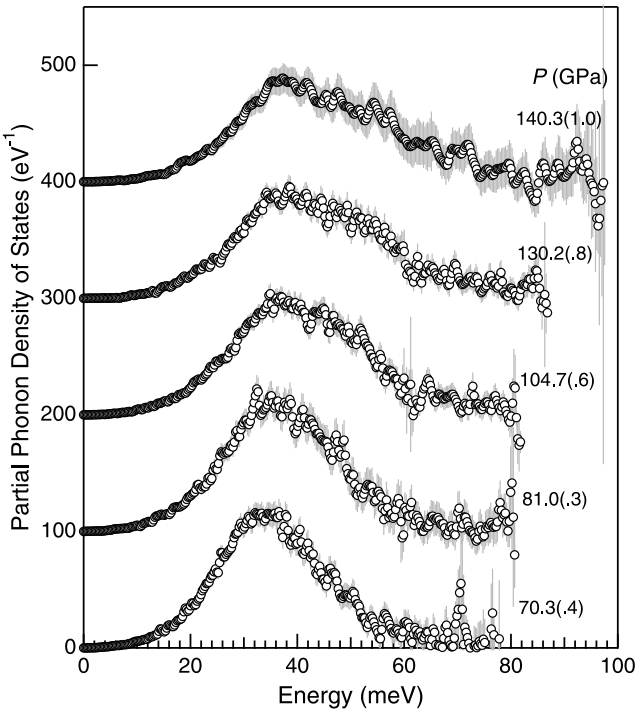

Figure 3. Partial phonon DOS of FP35 from 70 to 140 GPa at 300 K. With increasing pressure, the spectral features shift toward higher energies. The Debye sound velocity (V_D) at each pressure was derived from the low-energy region of the DOS.

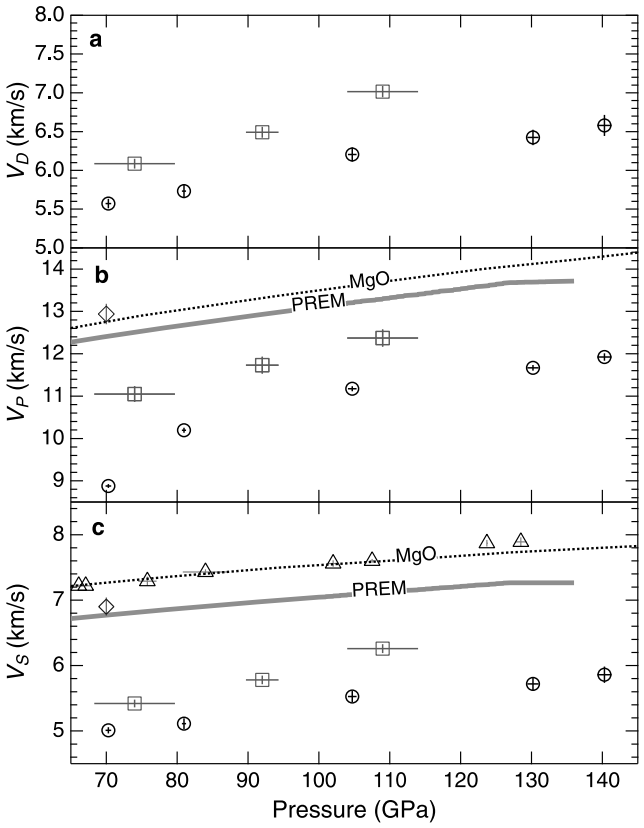

Figure 4. Sound velocities (a) V_D, (b) V_P, and (c) V_S of MgO, $(Mg_{0.83}Fe_{0.17})O$, $(Mg_{0.75}Fe_{0.25})O$, and FP35 from 70 to 140 GPa. Open triangles, MgO, from Brillouin spectroscopy combined with synchrotron XRD [*Murakami et al.*, 2009]; open diamonds, $(Mg_{0.83}Fe_{0.17})O$, from momentum-resolved inelastic x-ray scattering [*Antonangeli et al.*, 2011]; open squares, $(Mg_{0.75}Fe_{0.25})O$, based on the DOS obtained by NRIXS as reported in *Lin et al.* [2006] and applying the spin crossover EOS formalism (this study) to fit the data for $(Mg_{0.83}Fe_{0.17})O$ in *Lin et al.* [2005] (scaled to correct density); open circles, FP35, based on the DOS measured by NRIXS and the spin crossover EOS (this study). Gray solid curves: PREM [*Dziewonski and Anderson*, 1981]. Dashed curves: MgO at 300 K [*Wentzcovitch et al.*, 2010].

[18] Based on the EOS for FP35 presented here, the spin crossover for FP35 occurs at $p_{tr} = 64 \pm 3$ GPa. The steep slope in the pressure-trend of V_P for FP35 at 70 GPa can be explained by the fact that FP35 is in the vicinity of a spin crossover (see Figure 4). We see that V_P for $(Mg_{0.75}Fe_{0.25})O$ (FP25) [*Lin et al.*, 2006] and FP35 are lower than that for MgO [*Murakami et al.*, 2009]. However, V_P for $(Mg_{0.83}Fe_{0.17})O$ (FP17) at 70 GPa is higher than that for MgO [*Antonangeli et al.*, 2011]. It's not clear yet if this is a compositional effect, as few studies have been conducted at these pressures. At $P > 70$ GPa, V_P and V_S of FP25 and FP35 increase at different rates. At 100 GPa, increasing Fe content in the lattice of (Mg,Fe)O lowers the V_S by 19% and 27% for FP25 and FP35, respectively, compared to MgO (see Figure 4).

4. Discussion

[19] The FP35 sample investigated here is thought to be representative of ferropericlase in equilibrium with an Al-poor silicate perovskite containing 10 mol% Fe at conditions near the top of the lower mantle, based on partitioning experiments using a multianvil apparatus [*Fei et al.*, 1991; *Irifune*, 1994]. However, with increasing pressure and temperature, the partitioning behavior of Fe into ferropericlase coexisting with Al-bearing and Al-free perovskite has been shown to increase [*Fei et al.*, 1996; *Fiquet et al.*, 2010; *Murakami et al.*, 2005; *Sinmyo et al.*, 2008; *Sakai et al.*, 2009; *van Westrenen et al.*, 2005]. In the lowermost 200 km of the lower mantle, Fe has also been shown to enter preferentially into ferropericlase, compared with perovskite and post-perovskite [e.g. *Auzende et al.*, 2008; *Kobayashi*, 2005; *Sakai et al.*, 2009]. Therefore, FP35 may exist in lower mantle assemblages with variable Al concentrations. One can see that due to FP35's large V_S and V_P reductions compared to PREM, the amount of FP35 throughout the deeper sections of the lower mantle would have to be very small. The exact amount is not possible to assess, because there is still insufficient data on how *P-T* affects V_S and V_P for FP35 and other candidate petrologic assemblages in the deep mantle.

[20] It is possible to use our new data to speculate on how the presence of FP35 in distinct regions of the deep mantle would affect seismic observations and geodynamic models. Large low shear velocity provinces (LLSVPs) are arguably the largest discrete structures in the mantle. Seismic and mineral physics data suggest LLSVPs are thermochemically distinct from the surrounding material [e.g., *Dziewonski et al.*, 2010; *Helmberger and Ni*, 2005; *Sun et al.*, 2009, 2010; *Wang and Wen*, 2007] and geodynamic models suggest plausible scenarios for their formation [e.g., *Garnero and McNamara*, 2008; *McNamara and Zhong*, 2004; *Schubert et al.*, 2004; *Tan and Gurnis*, 2005]. For example, given observed variations of δV_S and δV_P within the African LLSVP, and if the density anomaly at a given temperature is equal or greater than ambient, then K_S must be larger than that of ambient mantle to maintain neutral buoyancy [e.g., *Tan and Gurnis*, 2005, 2007]. The presence of FP35 would

Table 2. Sound Velocities of FP35 From 70 to 140 GPa at 300 K[a]

ρ (g/cm^3)	P[b] (GPa)	V_D (km/s)	V_P (km/s)	V_S (km/s)	G (GPa)	K_S[c] (GPa)
5.881(.041)	70.3(.4)[d]	5.558(.059)	8.877(.046)	5.009(.048)	147.6(2.8)	266.7
6.071(.042)	81.0(.3)[d]	5.719(.088)	10.193(.059)	5.111(.082)	158.6(5.1)	419.3
6.392(.044)	104.7(.6)[d]	6.189(.090)	11.175(.061)	5.527(.084)	195.2(6.0)	537.9
6.706(.046)	130.2(.8)	6.409(.098)	11.667(.067)	5.720(.092)	219.4(7.1)	620.2
6.798(.047)	140.3(1.0)	6.565(.133)	11.922(.087)	5.860(.125)	233.4(9.9)	655.0

[a]Numbers in parentheses are the uncertainties.
[b]Pressures and associated uncertainties were determined from *in situ* XRD measurements based on the EOS of FP35 (this study).
[c]K_S can be approximated by K_T of FP35, because $K_S = K_T(1 + \alpha\gamma T)$ and $\alpha\gamma T < 0.01$ at room temperature.
[d]For these measurements, neon was loaded as the pressure transmitting medium.

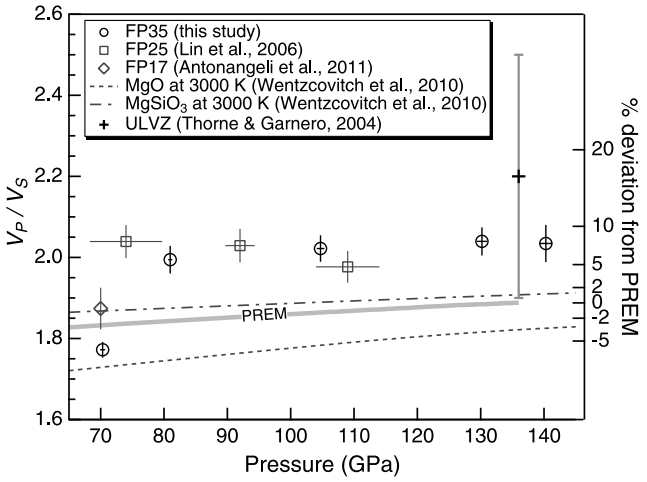

Figure 5. The ratio of V*P* to V*S* for (Mg,Fe)O at 300 K compared with PREM, ULVZs, theoretical calculations for $MgSiO_3$ and MgO at 3000 K [*Wentzcovitch et al.*, 2010].

enhance the density of the structure and at the pressures of the CMB region, LS FP35 at 300 K has a similar bulk modulus as PREM. However, temperature is likely to reduce the bulk modulus of FP35 at CMB conditions. Therefore, based on our data for the bulk and shear elastic properties of FP35 and the dynamic scenarios in *Tan and Gurnis* [2005, 2007], an enhanced content of FP35, or any Fe-rich (Mg,Fe)O, would likely not allow a large structure to maintain neutral buoyancy.

[21] The V_P/V_S of FP35 at 140 GPa and 300 K is ~2.03 (±0.06), which is higher than that reported for PREM and silicates, but at the lower end of reported values for ULVZ terrains [*Thorne and Garnero*, 2004] (see Figure 5). For example, if FP35 were used to explain some of the extreme shear wave reductions in ULVZs (−30% V_S) [e.g., *Garnero and Helmberger*, 1995; *McNamara et al.*, 2010], then this would require approximately a 50-50 mixture of FP35 and silicates. Such a large proportion of FP35 would suggest an extremely different chemistry for ULVZs than the surrounding mantle. This situation appears highly unlikely. Further, the corresponding reduction in V_P would be about −20%, which has been observed in some regions, but is not common [e.g. *Bower et al.*, 2011]. However, small amounts (~10%) of FP35 mixed with silicates at the CMB could explain moderate reductions in wave speeds and approximately +0.5% increase in density compared with PREM. The small, but positive, difference in density compared to ambient mantle would likely lead to dynamic structures that are triangular in shape and involve some entrainments [e.g., *Bower et al.*, 2011].

5. Conclusions

[22] A new spin crossover EOS has been presented to describe the *P-V* relation for FP35 through the HS-LS crossover. In the calculation of the single compression curve, we varied the zero-pressure volume, bulk modulus and its pressure derivative of the HS and LS states, and the transition parameter. We combined this spin crossover EOS with the measured partial phonon DOS and *in situ* XRD measurements of FP35 to derive V_S and V_P for LS FP35. Based on our measurements, we conclude that the presence of LS FP35 is unlikely to explain the seismic and dynamic features of LLSVPs. In regions of extreme shear wave speed reductions (−30% V_S) near the CMB, the terrain would have to contain ~50% FP35. This amount of FP35 is unlikely and would have a high buoyancy number, producing features that are essentially flat on top of the CMB [*Bower et al.*, 2011]. However, small amounts of FP35 (<10%) mixed with silicates could explain moderate reductions in wave speeds near the CMB.

[23] **Acknowledgments.** We thank J. Yan for help with the experimental set-up at the ALS and D. J. Bower for helpful discussions. The authors are grateful to NSF-EAR-CAREER-0956166, the Texaco postdoctoral fellowship from Caltech (to B.C.), and Keck Institute for Space Studies for support of this work. Sector 3 operations, beamline 12.2.2 and the gas-loading facility are partially supported by COMPRES. Use of the Advanced Photon Source is supported by the U.S. DOE, Office of Science (DE-AC02-06CH11357). The Advanced Light Source is supported by the U.S. DOE, Office of Science (DE-AC02-05CH11231). Microprobe analyses were carried out at the Caltech GPS Division Analytical Facility (funded in part by the MRSEC Program of the NSF under DMR-0080065). We also thank two anonymous reviewers and the editors for their useful comments.

References

Angel, R. J. (2001), Equation of State, in *High-Pressure, High-Temperature Crystal Chemistry*, *Rev. Mineral. Geochem.*, vol. 41, edited by R. M. Hazen and R. T. Downs, pp. 35–60, Mineral. Soc. of Am., Washington, D. C.

Antonangeli, D., J. Siebert, C. M. Aracne, D. L. Farber, A. Bosak, M. Hoesch, M. Krisch, F. J. Ryerson, G. Fiquet, and J. Badro (2011), Spin crossover in ferropericlase at high pressure: A seismologically transparent transition?, *Science*, *331*(6013), 64–67.

Auzende, A. L., J. Badro, F. J. Ryerson, P. K. Weber, S. J. Fallon, A. Addad, J. Siebert, and G. Fiquet (2008), Element partitioning between magnesium silicate perovskite and ferropericlase: New insights into bulk lower-mantle geochemistry, *Earth Planet. Sci. Lett.*, *269*(1–2), 164–174.

Badro, J., G. Fiquet, F. Guyot, J. Rueff, V. V. Struzhkin, G. Vanko, and G. Monaco (2003), Iron partitioning in Earth's mantle: Toward a deep lower mantle discontinuity, *Science*, *300*(5620), 789–791, doi:10.1126/science.1081311.

Bower, D. J., M. Gurnis, J. M. Jackson, and W. Sturhahn (2009), Enhanced convection and fast plumes in the lower mantle induced by the spin transition in ferropericlase, *Geophys. Res. Lett.*, *36*, L10306, doi:10.1029/2009GL037706.

Bower, D. J., J. K. Wicks, M. Gurnis, and J. M. Jackson (2011), A geodynamic and mineral physics model of a solid-state ultralow-velocity zone, *Earth Planet. Sci. Lett.*, *303*(3–4), 193–202.

Crowhurst, J. C., A. F. Goncharov, and J. M. Zaug (2004), Impulsive stimulated light scattering from opaque materials at high pressure, *J. Phys. Condens. Matter*, *16*(14), 1137–1142.

Crowhurst, J. C., J. M. Brown, A. F. Goncharov, and S. D. Jacobsen (2008), Elasticity of (Mg,Fe)O through the spin transition of iron in the lower mantle, *Science*, *319*(5862), 451–453.

Dziewonski, A. M., and D. L. Anderson (1981), Preliminary reference Earth model, *Phys. Earth Planet. Inter.*, *25*, 297–356.

Dziewonski, A. M., V. Lekic, and B. A. Romanowicz (2010), Mantle anchor structure: An argument for bottom up tectonics, *Earth Planet. Sci. Lett.*, *299*, 69–79.

Fei, Y., H.-K. Mao, and B. O. Mysen (1991), Experimental-determination of element partitioning and calculation of phase-relations in the MgO-FeO-SiO_2 system at high-pressure and high-temperature, *J. Geophys. Res.*, *96*(B2), 2157–2169.

Fei, Y., H.-K. Mao, J. Shu, and J. Hu (1992), $P - V - T$ equation of state of magnesiowüstite ($Mg_{0.6}Fe_{0.4}$)O, *Phys. Chem. Miner.*, *18*(7), 416–422.

Fei, Y., Y. Wang, and L. W. Finger (1996), Maximum solubility of FeO in (Mg,Fe)SiO_3-perovskite as a function of temperature at 26 GPa: Implication for FeO content in the lower mantle, *J. Geophys. Res.*, *101*(B5), 11,525–11,530.

Fei, Y., L. Zhang, A. Corgne, H. Watson, A. Ricolleau, Y. Meng, and V. Prakapenka (2007), Spin transition and equations of state of (Mg,

Fe)O solid solutions, *Geophys. Res. Lett.*, *34*, L17307, doi:10.1029/2007GL030712.
Fiquet, G., A. L. Auzende, J. Siebert, A. Corgne, H. Bureau, H. Ozawa, and G. Garbarino (2010), Melting of peridotite to 140 gigapascals, *Science*, *329*(5998), 1516–1518.
Garnero, E. J., and D. V. Helmberger (1995), A very slow basal layer underlying large-scale low-velocity anomalies in the lower mantle beneath the pacific: Evidence from core phases, *Phys. Earth Planet. Inter.*, *91*(1–3), 161–176.
Garnero, E. J., and A. K. McNamara (2008), Structure and dynamics of Earth's lower mantle, *Science*, *320*(5876), 626–628.
Goncharov, A. F., V. V. Struzhkin, and S. D. Jacobsen (2006), Reduced radiative conductivity of low-spin (Mg, Fe) O in the lower mantle, *Science*, *312*(5777), 1205–1207.
Helmberger, D. V., and S. Ni (2005), Seismic modeling constraints on the south African super plume, in *Earth's Deep Mantle: Structure, Composition, and Evolution*, *Geophys. Monogr. Ser.*, vol. 160, edited by R. D. van der Hilst et al., pp. 63–81, AGU, Washington, D. C.
Irifune, T. (1994), Absence of an aluminous phase in the upper part of the Earth's lower mantle, *Nature*, *370*(6485), 131–133.
Jackson, J. M., J. Zhang, and J. D. Bass (2004), Sound velocities and elasticity of aluminous $MgSiO_3$ perovskite: Implications for aluminum heterogeneity in Earth's lower mantle, *Geophys. Res. Lett.*, *31*, L10614, doi:10.1029/2004GL019918.
Jackson, J. M., S. V. Sinogeikin, S. D. Jacobsen, H. J. Reichmann, S. J. Mackwell, and J. D. Bass (2006), Single-crystal elasticity and sound velocities of $(Mg_{0.94}Fe_{0.06})O$ ferropericlase to 20 GPa, *J. Geophys. Res.*, *111*, B09203, doi:10.1029/2005JB004052.
Jackson, J. M., E. A. Hamecher, and W. Sturhahn (2009), Nuclear resonant X-ray spectroscopy of $(Mg,Fe)SiO_3$ orthoenstatites, *Eur. J. Mineral.*, *21*(3), 551–560.
Jacobsen, S. D., H. J. Reichmann, H. A. Spetzler, S. J. Mackwell, J. R. Smyth, R. J. Angel, and C. A. McCammon (2002), Structure and elasticity of single-crystal (Mg, Fe)O and a new method of generating shear waves for gigahertz ultrasonic interferometry, *J. Geophys. Res.*, *107*(B2), 2037, doi:10.1029/2001JB000490.
Jacobsen, S. D., C. M. Holl, K. A. Adams, R. A. Fischer, E. S. Martin, C. R. Bina, J. Lin, V. B. Prakapenka, A. Kubo, and P. Dera (2008), Compression of single-crystal magnesium oxide to 118 GPa and a ruby pressure gauge for helium pressure media, *Am. Mineral.*, *93*(11–12), 1823–1828, doi:10.2138/am.2008.2988.
Kobayashi, Y., T. Kondo, E. Ohtani, N. Hirao, N. Miyajima, T. Yagi, T. Nagase, and T. Kikegawa (2005), Fe-Mg partitioning between $(Mg, Fe)SiO_3$ post-perovskite, perovskite, and magnesiowüstite in the Earth's lower mantle, *Geophys. Res. Lett.*, *32*, L19301, doi:10.1029/2005GL023257.
Komabayashi, T., K. Hirose, Y. Nagaya, E. Sugimura, and Y. Ohishi (2010), High-temperature compression of ferropericlase and the effect of temperature on iron spin transition, *Earth Planet. Sci. Lett.*, *297*(3–4), 691–699, doi:10.1016/j.epsl.2010.07.025.
Lin, J.-F., J. Shu, H.-K. Mao, R. J. Hemley, and G. Shen (2003), Amorphous boron gasket in diamond anvil cell research, *Rev. Sci. Instr.*, *74*, 4732.
Lin, J.-F., V. V. Struzhkin, S. D. Jacobsen, M. Y. Hu, P. Chow, J. Kung, H. Liu, H.-K. Mao, and R. J. Hemley (2005), Spin transition of iron in magnesiowustite in the Earth's lower mantle, *Nature*, *436*, 377–380, doi:10.1038/nature03825.
Lin, J.-F., S. D. Jacobsen, W. Sturhahn, J. M. Jackson, J.-C. Zhao, and C.-S. Yoo (2006), Sound velocities of ferropericlase in the Earth's lower mantle, *Geophys. Res. Lett.*, *33*, L22304, doi:10.1029/2006GL028099.
Mao, Z., J.-F. Lin, J. Liu, and V. B. Prakapenka (2011), Thermal equation of state of lower-mantle ferropericlase across the spin crossover, *Geophys. Res. Lett.*, *38*, L23308, doi:10.1029/2011GL049915.
Marquardt, H., S. Speziale, H. J. Reichmann, D. J. Frost, F. R. Schilling, and E. J. Garnero (2009), Elastic shear anisotropy of ferropericlase in Earth's lower mantle, *Science*, *324*(5924), 224–226.
Mattern, E., J. Matas, Y. Ricard, and J. Bass (2005), Lower mantle composition and temperature from mineral physics and thermodynamic modelling, *Geophys. J. Int.*, *160*, 973–990, doi:10.1111/j.1365-246X.2004.02549.x.
McNamara, A. K., and S. Zhong (2004), Thermochemical structures within a spherical mantle: Superplumes or piles, *J. Geophys. Res.*, *109*, B07402, doi:10.1029/2003JB002847.
McNamara, A. K., E. J. Garnero, and S. Rost (2010), Tracking deep mantle reservoirs with ultra-low velocity zones, *Earth Planet. Sci. Lett.*, *299*(1), 1–9.
Murakami, M., and J. D. Bass (2011), Evidence of denser $MgSiO_3$ glass above 133 gigapascal (GPa) and implications for remnants of ultradense silicate melt from a deep magma ocean, *Proc. Natl. Acad. Sci. U. S. A.*, *108*(42), 17,286–17,289.
Murakami, M., K. Hirose, N. Sata, and Y. Ohishi (2005), Post-perovskite phase transition and mineral chemistry in the pyrolitic lowermost mantle, *Geophys. Res. Lett.*, *32*, L03304, doi:10.1029/2004GL021956.
Murakami, M., S. V. Sinogeikin, J. D. Bass, N. Sata, Y. Ohishi, and K. Hirose (2007a), Sound velocity of $MgSiO_3$ post-perovskite phase: A constraint on the D″ discontinuity, *Earth Planet. Sci. Lett.*, *259*(1–2), 18–23.
Murakami, M., S. V. Sinogeikin, H. Hellwig, J. D. Bass, and J. Li (2007b), Sound velocity of $MgSiO_3$ perovskite to Mbar pressure, *Earth Planet. Sci. Lett.*, *256*(1–2), 47–54, doi:10.1016/j.epsl.2007.01.011.
Murakami, M., Y. Ohishi, N. Hirao, and K. Hirose (2009), Elasticity of MgO to 130 GPa: Implications for lower mantle mineralogy, *Earth Planet. Sci. Lett.*, *277*(1–2), 123–129.
Rivers, M., V. B. Prakapenka, A. Kubo, C. Pullins, C. M. Holl, and S. D. Jacobsen (2008), The COMPRES/GSECARS gas-loading system for diamond anvil cells at the Advanced Photon Source, *High Pressure Res.*, *28*(3), 273–292, doi:10.1080/08957950802333593.
Sakai, T., E. Ohtani, H. Terasaki, M. Miyahara, M. Nishijima, N. Hirao, Y. Ohishi, and N. Sata (2009), Fe–Mg partitioning between post-perovskite and ferropericlase in the lowermost mantle, *Phys. Chem. Miner.*, *37*(487–496), 1–10.
Schubert, G., G. Masters, P. Olson, and P. Tackley (2004), Superplumes or plume clusters?, *Phys. Earth Planet. Inter.*, *146*(1–2), 147–162.
Sinmyo, R., K. Hirose, D. Nishio-Hamane, Y. Seto, K. Fujino, N. Sata, and Y. Ohishi (2008), Partitioning of iron between perovskite/postperovskite and ferropericlase in the lower mantle, *J. Geophys. Res.*, *113*, B11204, doi:10.1029/2008JB005730.
Speziale, S., A. Milner, V. E. Lee, S. M. Clark, M. P. Pasternak, and R. Jeanloz (2005), Iron spin transition in Earth's mantle, *Proc. Natl. Acad. Sci. U. S. A.*, *102*(50), 17,918–17,922, doi:10.1073/pnas.0508919102.
Sturhahn, W. (2000), CONUSS and PHOENIX: Evaluation of nuclear resonant scattering data, *Hyperfine Interact.*, *125*(1), 149–172.
Sturhahn, W. (2004), Nuclear resonant spectroscopy, *J. Phys. Condens. Matter*, *16*(5), 497–530.
Sturhahn, W., and J. M. Jackson (2007), Geophysical applications of nuclear resonant spectroscopy, *Spec. Pap. Geol. Soc. Am.*, *421*, 157–174, doi:10.1130/2007.2421(09).
Sturhahn, W., and V. G. Kohn (1999), Theoretical aspects of incoherent nuclear resonant scattering, *Hyperfine Interact.*, *123*(1–8), 367–399.
Sturhahn, W., J. M. Jackson, and J.-F. Lin (2005), The spin state of iron in minerals of the Earth's lower mantle, *Geophys. Res. Lett.*, *32*, L12307, doi:10.1029/2005GL022802.
Sun, D., D. Helmberger, S. Ni, and D. Bower (2009), Direct measures of lateral velocity variation in the deep Earth, *J. Geophys. Res.*, *114*, B05303, doi:10.1029/2008JB005873.
Sun, D., D. Helmberger, and M. Gurnis (2010), A narrow, mid-mantle plume below southern Africa, *Geophys. Res. Lett.*, *37*, L09302, doi:10.1029/2009GL042339.
Tan, E., and M. Gurnis (2005), Metastable superplumes and mantle compressibility, *Geophys. Res. Lett.*, *32*, L20307, doi:10.1029/2005GL024190.
Tan, E., and M. Gurnis (2007), Compressible thermochemical convection and application to lower mantle structures, *J. Geophys. Res.*, *112*, B06304, doi:10.1029/2006JB004505.
Thorne, M. S., and E. J. Garnero (2004), Inferences on ultralow-velocity zone structure from a global analysis of SPdKS waves, *J. Geophys. Res.*, *109*, B08301, doi:10.1029/2004JB003010.
Toellner, T. S. (2000), Monochromatization of synchrotron radiation for nuclear resonant scattering experiments, *Hyperfine Interact.*, *125*(1–4), 3–28.
van Westrenen, W., et al. (2005), Thermoelastic properties of $(Mg_{0.64}Fe_{0.36})O$ ferropericlase based on in situ X-ray diffraction to 26.7 GPa and 2173K, *Phys. Earth Planet. Inter.*, *151*(1–2), 163–176.
Wang, Y., and L. Wen (2007), Geometry and P and S velocity structure of the "African Anomaly," *J. Geophys. Res.*, *112*, B05313, doi:10.1029/2006JB004483.
Wentzcovitch, R. M., J. F. Justo, Z. Wu, C. R. S. da Silva, D. A. Yuen, and D. Kohlstedt (2009), Anomalous compressibility of ferropericlase throughout the iron spin cross-over, *Proc. Natl. Acad. Sci. U. S. A.*, *106*(21), 8447–8452.
Wentzcovitch, R. M., Z. Wu, and P. Carrier (2010), First principles quasi-harmonic thermoelasticity of mantle minerals, *Rev. Mineral. Geochem.*, *71*(1), 99–128.
Wicks, J. K., J. M. Jackson, and W. Sturhahn (2010), Very low sound velocities in iron-rich (Mg, Fe)O: Implications for the core-mantle boundary region, *Geophys. Res. Lett.*, *37*, L15304, doi:10.1029/2010GL043689.

Wu, Z., J. F. Justo, C. R. S. da Silva, S. de Gironcoli, and R. M. Wentzcovitch (2009), Anomalous thermodynamic properties in ferropericlase throughout its spin crossover, *Phys. Rev. B*, *80*(1), 014409, doi:10.1103/PhysRevB.80.014409.

Zhuravlev, K. K., J. M. Jackson, A. S. Wolf, J. K. Wicks, J. Yan, and S. M. Clark (2009), Isothermal compression behavior of (Mg,Fe)O using neon as a pressure medium, *Phys. Chem. Miner.*, *37*(7), 465–474, doi:10.1007/s00269-009-0347-6.